Online Research @ Cardiff

information services
gwasanaethau gwybodaeth

Polarity determination of crystal defects in zincblende GaN by aberration-corrected electron microscopy

Huixin Xiu, Simon M. Fairclough, Abhiram Gundimeda, et al.

ARTICLES YOU MAY BE INTERESTED IN

Cubic GaN and InGaN/GaN quantum wells
Applied Physics Reviews **9**, 041309 (2022); https://doi.org/10.1063/5.0097558

Formation of a-type dislocations near the InGaN/GaN interface during post-growth processing of epitaxial structures
Journal of Applied Physics **133**, 045304 (2023); https://doi.org/10.1063/5.0128514

High conductivity and low activation energy in p-type AlGaN
Applied Physics Letters **122**, 092103 (2023); https://doi.org/10.1063/5.0141863

Polarity determination of crystal defects in zincblende GaN by aberration-corrected electron microscopy

View Online   Export Citation   CrossMark

Huixin Xiu,[1,2] 🆔 Simon M. Fairclough,[2] 🆔 Abhiram Gundimeda,[2] 🆔 Menno J. Kappers,[2] 🆔 David J. Wallis,[2,3] 🆔
Rachel A. Oliver,[2] 🆔 and Martin Frentrup[2,a)] 🆔

AFFILIATIONS

[1]School of Materials and Chemistry, University of Shanghai for Science and Technology, 516 Jungong Road, Yangpu District, Shanghai 200093, China
[2]Department of Materials Science and Metallurgy, University of Cambridge, 27 Charles Babbage Rd., Cambridge CB3 0FS, United Kingdom
[3]Centre for High Frequency Engineering, University of Cardiff, 5 The Parade, Newport Road, Cardiff CF24 3AA, United Kingdom

[a)]Author to whom correspondence should be addressed: mf562@cam.ac.uk

ABSTRACT

Aberration-corrected scanning transmission electron microscopy techniques are used to study the bonding configuration between gallium cations and nitrogen anions at defects in metalorganic vapor-phase epitaxy-grown cubic zincblende GaN on vicinal (001) 3C-SiC/Si. By combining high-angle annular dark-field and annular bright-field imaging, the orientation and bond polarity of planar defects, such as stacking faults and wurtzite inclusions, were identified. It is found that the substrate miscut direction toward one of the 3C-SiC ⟨110⟩ in-plane directions is correlated with the crystallographic [1–10] in-plane direction and that the {111} planes with a zone axis parallel to the miscut have a Ga-polar character, whereas the {111} planes in the zone perpendicular to the miscut direction have N-polarity. The polarity of {111}-type stacking faults is maintained in the former case by rotating the coordination of Ga atoms by 180° around the ⟨111⟩ polar axes and in the latter case by a similar rotation of the coordination of the N atoms. The presence of small amounts of the hexagonal wurtzite phase on Ga-polar {111} planes and their total absence on N-polar {111} planes is tentatively explained by the preferential growth of wurtzite GaN in the [0001] Ga-polar direction under non-optimized growth conditions.

I. INTRODUCTION

Cubic zincblende (zb) III-nitrides grown in the (001) orientation are technologically promising semiconductor materials due to the absence of polarization fields and the associated unwanted quantum-confined Stark effect when strained biaxially,[1] their smaller bandgaps compared to the commonly used hexagonal wurtzite (wz) phases,[2] and their high hole mobility.[3,4] These exceptional material properties make them suitable candidates for efficient green wavelength LEDs[5] and high frequency transistor applications,[6–8] although early devices have not yet reached the performance of their hexagonal counterparts. One explanation for this shortcoming in efficiency is related to the metastable nature of

zb-GaN and its alloys, which leads to a rich microstructure with a high density of {111}-type stacking faults (SFs), twinned regions, and wz inclusions when grown on foreign cubic substrates, like GaAs (001),[9] 3C-SiC/Si (001),[10,11] and Si (001).[12] These defects and polytypism can potentially impair the functionality of devices,[13,14] and, therefore, further optimization of the growth conditions[11,15] is required to suppress their formation. Furthermore, it has previously been shown that a substrate miscut of a few degrees [required to avoid the formation of anti-phase domains when zb-GaN is grown on 3C-SiC/Si (001) or Si (001)[11]], has a profound effect on the density and distribution of SFs.[16]

To understand the growth challenges of zb-GaN, which is a partially ionic crystal with tetrahedrally coordinated bonding

geometry, it is important to take into account the polarity of the bonds between metal cations and nitrogen anions. This bond polarity arises from the large difference in the electronegativity of the components (1.81 for gallium compared to 3.04 for nitrogen on the Pauling scale)[17] and the lack of an inversion symmetry in both the zb and the wz structures. To differentiate between the two opposing directions parallel to the polar bonds, the direction pointing from a gallium (Ga) to a nitrogen (N) atom is commonly designated as Ga-faced, Ga-polar, or A-type, whereas the opposite direction is named as N-faced, N-polar, or B-type.[18]

The polarity of the bonds has a crucial role in the growth of the material, such as the defect density as well as the surface and interface roughness,[19–21] leading to profound consequences for the properties and performance of multilayer heterostructure devices made of them. For example, N-polar (000-1) wz-GaN and AlGaN layers tend to grow with an increased surface and interface roughness compared to Ga-polar samples,[20,21] which can impair the performance of N-polar AlGaN devices.[21] On the other hand, wz N-polar (000-1) InGaN samples with a high In content have a higher thermal stability compared to III-polar InGaN, making such a growth appealing for long wavelength nitride-based LED applications.[22] Furthermore, the polarity has a strong influence on the growth of nanostructures, like GaN nanowires,[23] and the incorporation of impurities.[24]

Next, we consider the potential impact of bond polarity on the less well-explored case of the zincblende GaN system. Previous x-ray diffraction (XRD) studies (Ref. 10 and references therein) have confirmed that the crystallographic relation between the zb matrix and unwanted wz inclusions is $(111)_{zb} \parallel (0001)_{wz}$, with $[-110]_{zb} \parallel [1-210]_{wz}$ for two of the four inequivalent $\{111\}_{zb}$ facets. As the closed-packed planes are parallel to each other and differ only in the stacking sequence, it is evident that structural phase-transition from the zb to wz phase is associated with the presence of planar defects along the $\{111\}$ planes. In view of the opposing polarity of the four $\{111\}_{zb}$ facets, $(0001)_{wz}$ stacking does not necessarily occur with equal probability on each of them, leading to complex microstructures.

To study the polarity of semiconductor thin films at a microscopic scale, a range of microscopy techniques have been extensively used and discussed in the literature[19,25–28] of which convergent beam electron diffraction (CBED) in transmission electron microscopy is one of the most commonly used. However, CBED is not suitable for analyses on the atomic scale as it requires the measurement of a relatively large volume of material from specimens of typically more than 100 nm thickness to collect diffraction data, to allow matching to simulated patterns of possible crystal orientations.

In the present study, we use a combination of high-angle annular dark-field (HAADF) and annular bright-field (ABF) imaging based on aberration-corrected scanning transmission electron microscopy (STEM) to study individual defects and small volume wz and twin inclusions directly in a zb-GaN thin film grown on (001) 3C-SiC/Si. The strength of the combined HAADF and ABF STEM techniques in the imaging of a light element such as nitrogen in GaN and, therefore, the polarity assignment of the layers was illustrated by De la Mata and colleagues for an undefective material.[29] Here, we extend the application of this technique to imaging the bond polarity in defects in zincblende GaN and, thus, investigate how polarity may influence the likelihood of formation of such defects.

II. EXPERIMENTAL METHODS

Because aberration-corrected STEM requires the preparation of ultra-thin specimens, which can only be realized in a highly localized area, a zb-GaN on 3C-SiC sample has been chosen for which x-ray diffraction has previously revealed a very high zb phase purity to avoid imaging the projection of multiple SF bunches and wurtzite inclusions.

The zb-GaN sample investigated in this work was grown by metalorganic vapor-phase epitaxy (MOVPE) on a (001) 3C-SiC/Si template with a 4° miscut toward one of the ⟨110⟩ in-plane directions. After the nitridation of the 3C-SiC/Si template at 960 °C and deposition of a 40 nm-thick low-temperature GaN nucleation layer grown at about 600 °C, the ~380 nm-thick zb-GaN epilayer was grown at a temperature of 875 °C and a V/III ratio of 76 in a hydrogen ambient. This sample has a zb phase purity of above 98%,[11] and a sample grown under similar conditions has previously been examined in detail in TEM, revealing only a few isolated wurtzite inclusions and a strong anisotropy in the SF distribution relative to the miscut.[16]

In order to investigate the polarity and orientation of individual defects in the zb-GaN epilayer, two cross-sectional TEM lamellae have been prepared with the zone axis either (1) perpendicular or (2) parallel to the miscut direction, as illustrated in Fig. 1 in blue and red, respectively. For this purpose, a standard lift-out technique in a Thermo Fisher Scientific™ Helios unicolor (UC) dual beam microscope with a focused ion beam (FIB) column was used, for which first a 2–3 μm-thick Pt protection layer was added to the sample surface via electron beam deposition followed by Ga
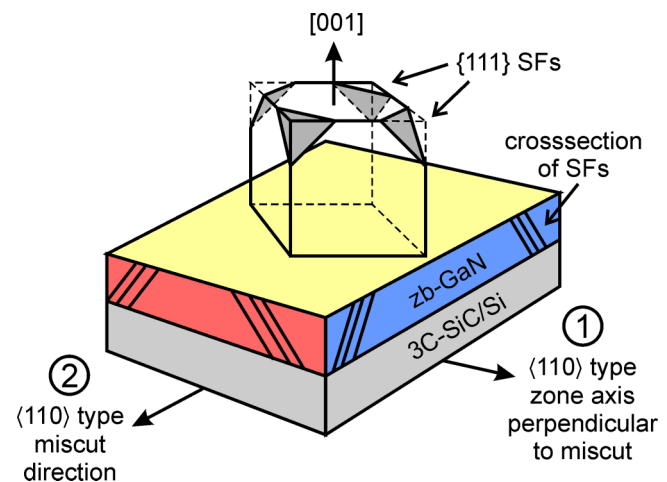

FIG. 1. Schematic showing a zb-GaN film on top of a 3C-SiC/Si substrate with a 4° miscut toward one of the two ⟨110⟩ in-plane directions. The unit cell illustrates the orientation of the four different $\{111\}$ SF types, while the blue and red colored areas show the zones for which TEM lamellae have been prepared.

deposition. Trenches on either side of the regions of interest were milled using a 30 kV Ga^{3+} ion beam and lifted out using an OmniProbe manipulator. The samples were then transferred onto copper grids to be further milled to a thickness of 100 nm or less, with the final milling condition set at a low voltage of 2 kV. The specimen with the zone axis perpendicular to the miscut direction underwent an additional post-cleaning using Ar^+ ions in a Fischione NanoMill® system to remove contaminations from long storage between lamellae preparation and subsequent electron microscopic characterization.

STEM annular bright-field (ABF) and high-angle annular dark-field (HAADF) images were acquired simultaneously in a Thermo Fisher Scientific™ Titan Themis Probe-corrected (S) TEM operated at 300 kV, using a segmented DF4 detector for ABF imaging and a HAADF detector for HAADF imaging. To achieve the highest resolution, the STEM convergence angle was selected as 23.5 mrad and the collection angle was set to 45–200 mrad for HAADF images and 11–42 mrad for ABF images, while a very low electron beam current between 40 and 100 pA was used for sample examination. To enable easy interpretation of the combined ABF and HAADF data sets, color coded images were constructed.

III. RESULTS AND DISCUSSION

A. Polarity in the zone perpendicular to the miscut direction (1)

First, we will investigate the polarity of crystal defects in the zone perpendicular to the miscut direction; i.e., in reference to
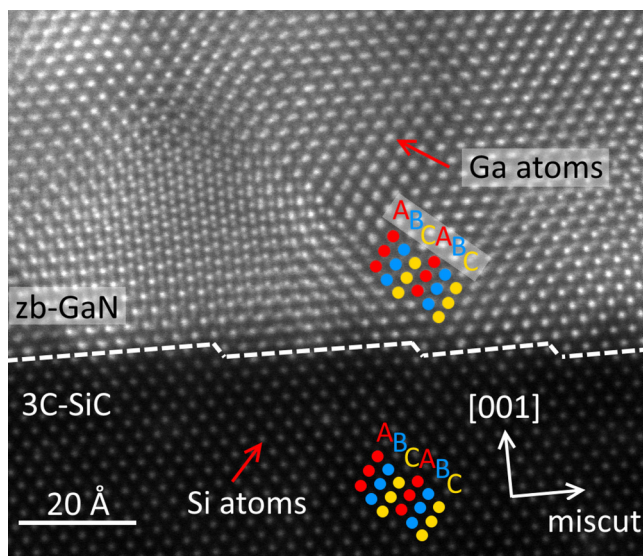

FIG. 2. HAADF STEM image viewed normal to the miscut direction of a (001) zb-GaN layer grown on 3C-SiC. Only the heavy atomic columns Ga and Si are visible.

Fig. 1, a TEM foil was prepared of the blue colored area. Previous studies had revealed a strong anisotropy in the distribution of SFs aligned in opposite directions within this zone.[16]

Figure 2 shows a typical cross-sectional view of the interface between (001) oriented zb-GaN and 3C-SiC. As HAADF STEM is highly sensitive to heavy elements (with high Z-number), it only reveals the positions of gallium (Ga) and silicon (Si) atoms but not the positions of nitrogen (N) and carbon (C) atoms. In the SiC substrate as well as in the GaN thin film, the atoms form a characteristic ABCABC stacking of the {111} planes typical for the zb crystal structure. The interface appears to be almost atomically smooth with one-monolayer height steps, every few nanometers, which confirms that the view direction (zone axis) is perpendicular to the miscut direction.

The region of the sample area near the heterointerface is observed to contain a high density of {111}-type SFs (from both zones)[30] so that the impact of strain and the potential superposition of multiple defects are likely to impair the high resolution imaging required for the polarity analysis. Therefore, an area of the TEM specimen a few 100 nm away from the interface was chosen for more detailed examination. This area was specially thinned down to just a few tens of nm thickness during the specimen preparation so that it contains only a small number of defects. TEM images of this area are shown in Fig. 3.

Figure 3(a) shows a small section of a larger HAADF STEM image, displaying the position of heavy Ga atoms in the GaN lattice. The yellow dashed line indicates the position at which the natural zb stacking of {111} planes is interrupted with one plane missing so that the stacking order has changed to –ABC–**AB**–ABC–. This intrinsic SF (I-SF) has likely been formed at the zb-GaN/3C-SiC heterointerface by the dissociation of a perfect 60° misfit dislocation or is formed by the glide of a dislocation loop from the free surface.[30] To resolve the location of the much lighter N atoms (Z = 7), ABF STEM images were acquired simultaneously for the same specimen region in Fig. 3(b). Close to the Ga atomic columns, a faint contrast from N atomic columns is now visible. To increase the visibility and to allow study of the coordination of these elements, the ABF image and the HAADF image have been color coded and merged in Fig. 3(c), where Ga atomic columns appear as large orange circular structures and N atomic columns as small blue objects in front of a dark background. The resulting image shows three perfectly stacked zb-GaN regions, which are separated by two I-SFs on converging {111} planes. Figure 3(d) shows a magnified image of a perfect zb-GaN region. Comparison of the coordination of the Ga and N atoms with projections of the unit cell along [1–10] and [110] in Fig. 3(f) reveals that the STEM images display the [110] zone.

In the zb-region of the STEM image in Fig. 3(d), the structure can be envisaged of alternating {1–11} layers of each atom type (Ga and N). The orientation of the GaN dumbbell pairs normal to the {1–11} planes of this zone reveals that these planes are N-polar (when viewed from the GaN/3C-SiC interface further down the image, i.e., the bonds along [1–11] point from N to Ga atoms) as also highlighted by the overlaid schematics. This polarity is preserved at the I-SF. The overlaid schematic of the magnified image in Fig. 3(e) shows that directly at the I-SF plane (depicted by the yellow dash line), the coordination of the N atoms is rotated by
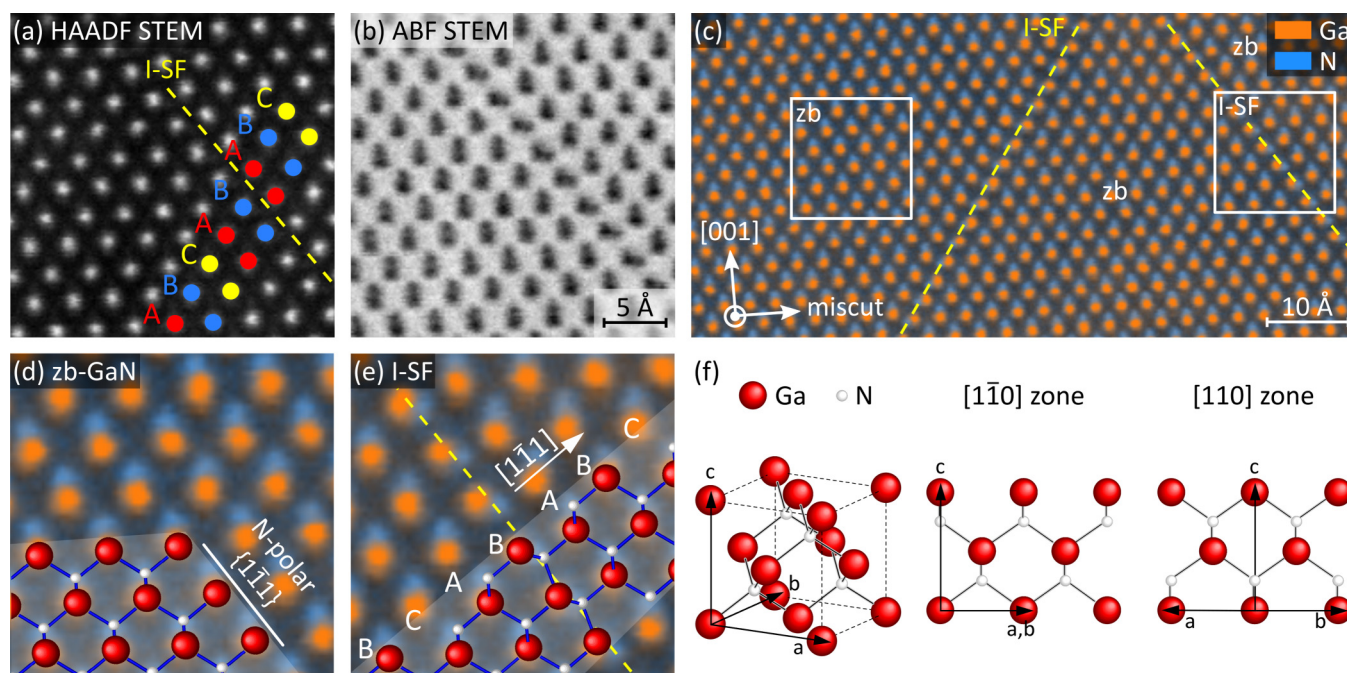
FIG. 3. Sections of an (a) HAADF STEM and (b) ABF STEM image of the same specimen region of the zb-GaN epilayer taken at the zone axis perpendicular to the miscut direction. (c) Combined full ABF STEM and HAADF STEM images showing the positions of Ga atomic columns in orange and the positions of the N atomic columns in blue. Magnified images of the white boxes are shown in (d) and (e). (f) 3D schematic of a zb-GaN unit cell and projection of the unit cell along [−110] and [110].

180° around the polar axis along [1–11]. (A sketch of the atomic arrangement in 3D is shown in the supplementary material.)

Interestingly, other than I-SFs, no extended regions with the wurtzite phase have been found in this zone—neither in the small sample area chosen for the polarization analysis nor in a larger region near the interface. This is in agreement with the more global analysis by x-ray diffraction, revealing that no signal is observed from wurtzite inclusions formed on {111} facets in the [110] zone perpendicular to the sample miscut, i.e., the blue colored plane in Fig. 1.

B. Polarity in the zone parallel to the miscut direction (2)

Next, we consider the polarity of the GaN bonds in the zone parallel to the substrate's miscut direction, depicted as the red colored plane in Fig. 1. The combined ABF-HAADF STEM image of this zone, taken from an area ~350 nm away from the interface, is shown in Fig. 4(a). Four distinct regions of interest can be identified. The large majority of the TEM foil shows a perfectly stacked zb phase of GaN. In between, local defective regions of wz-like stacking can be observed too. These include intrinsic SFs (I-SFs), an extrinsic SF (E-SF), and a diagonal band of wz-GaN. Figures 4(b)–4(e) show magnified images of these distinct structural features marked by the white boxes in (a).

In the projection on the zb-GaN region [Fig. 4(b)], Ga atomic columns appear to be located above the N atomic columns, shown in orange and blue, respectively. Comparing the arrangement of Ga and N atoms with the schematics in Fig. 3(f) allows us to identify the zone in Fig. 4 as [1–10]. In this zone, the bonds along [111] and [−1–11] point from Ga to N atoms, highlighting the Ga-polar character of the corresponding (111) and (−1–11) planes. At the I-SFs, as seen in Fig. 4(c), this Ga-polar character is maintained by rotating the coordination of the Ga metal atoms by 180° around the polar axis normal to the SF. (A 3D sketch of this rotation is shown in the supplementary material.) Both these observations are different from those made previously for the zone perpendicular to the miscut direction in Sec. III A and highlight the opposite polarity of the two sets of {111} planes.

Figures 4(d) and 4(e) show the arrangement of Ga and N atoms at an E-SF and a thin 4 ML-wide band of the wurtzite phase GaN, running across the zincblende region in the [1-10] zone. In contrast to the I-SF, the coordination of the Ga atoms in the E-SF changes the direction in two successive {111} GaN bilayers (instead of one bilayer) compared to the surrounding zincblende phase, which results in a –ABC–**BA**–BCA– stacking. This is also different to the wz inclusion, where the tetrahedral coordination of Ga atoms changes direction after each (0001) GaN bilayer to form the characteristic –ABAB– stacking of the wurtzite structure. However, for all these crystallographic defects in the [1–10] zone, the
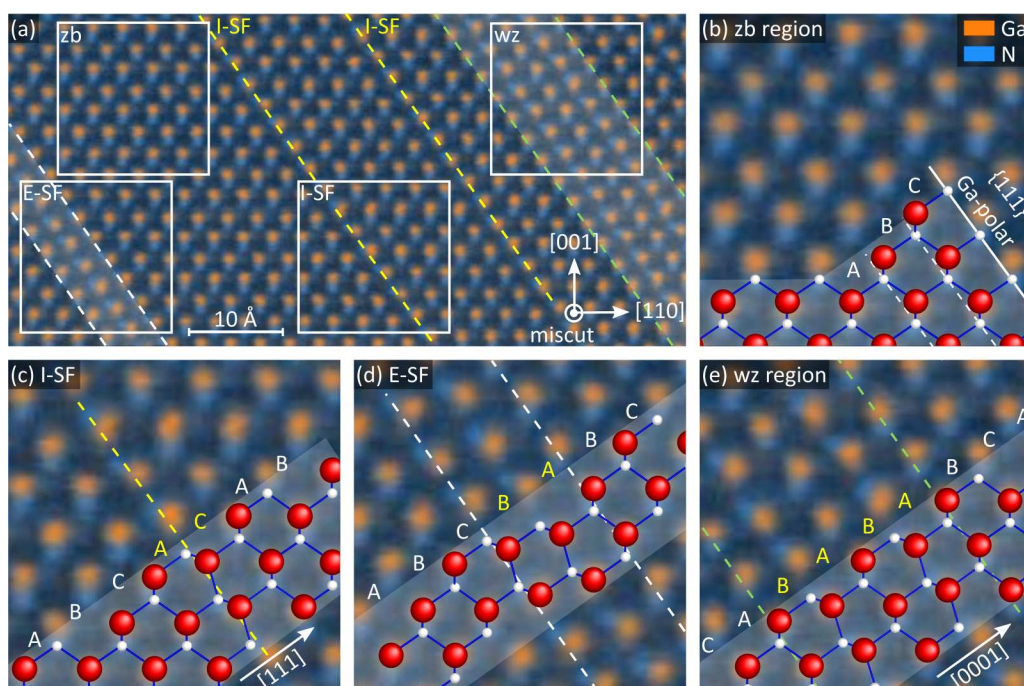
FIG. 4. (a) Combined ABF STEM and HAADF STEM image taken at the zone axis parallel to the miscut direction. The magnified regions show the positions of Ga (orange) and N (blue) atomic columns in the zb-region (b), near intrinsic SFs (c), at an extrinsic SF (2 ML thick twinned region) (d), and in a wurtzite region (e).
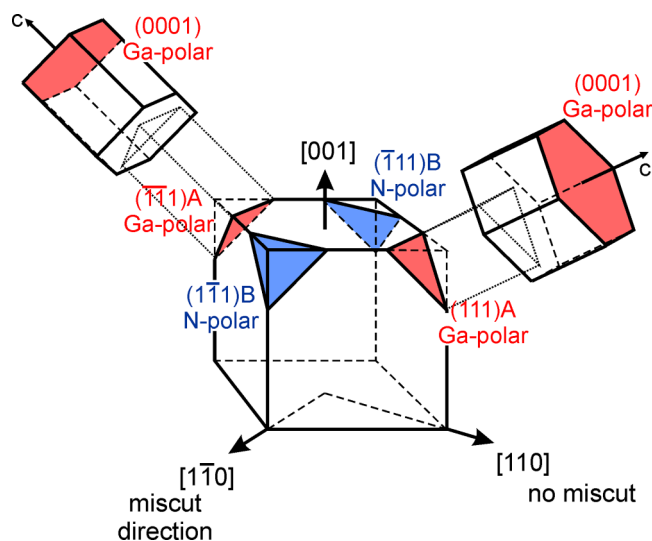

FIG. 5. Schematic of a (001) oriented cubic zb-GaN unit cell, showing the arrangement of {111} Ga-polar (red) and N-polar (blue) planes relative to the [1–10] miscut direction. Growth of (0001) Ga-polar wz inclusions is supported on the Ga-polar {111} zb-GaN planes.

Ga-polarity is preserved through the rotation of the coordination of Ga atoms rather than N atoms as it is for the [110] zone in Sec. III A.

C. Discussion

Figure 5 summarizes the findings of the TEM experiments. It shows schematically that the two {111} planes, which are visible edge-on in a TEM image with the zone axis parallel to the miscut direction (marked in red), have a Ga-polar character and facilitate the growth of wurtzite inclusions with the same polarity. On the other hand, the two {111} planes, which are visible edge-on in the micrograph with the [110] zone axis perpendicular to the miscut (marked in blue), have a N-polar character. Since the polarity is preserved at planar defects, wurtzite inclusions that would form on these latter planes would have a (000-1) N-polar character. The observation that wz inclusions are present in the former zone but absent in the latter (consistent with earlier XRD analysis indicating anisotropy in wurtzite formation[10]) could be explained by the different growth behavior of (000-1) N-polar and (0001) Ga-polar wz-GaN. The growth in the latter orientation at low V/III ratios has been observed to be faster than that in the N-polar direction.[31,32] It should, however, be noted that while these low V/III ratio growth conditions are similar to those used for cubic GaN in this study, the growth temperature for cubic zb-GaN is substantially

lower, rendering direct comparison difficult. Therefore, we infer that the growth of wurtzite inclusions is more likely on the Ga-polar {111} facets of the zb-GaN thin film. However, it is known that in wz-GaN epitaxy, it is possible to promote N-polar growth over Ga-polar growth.[25,33,34] Engineering the growth conditions in order to discourage Ga-polar growth would possibly help to suppress wz inclusions parallel to the Ga-polar {111} planes in zb-GaN thin films but risks promoting the growth of N-polar (000-1) wz-GaN parallel to the N-polar {111} zb-GaN planes. It is, therefore, of high importance for the development of high quality zb-GaN thin films to find and remain within the growth regime for which both wz orientations are either low in concentration and in good balance or even suppressed completely. This is consistent with our observation that the growth window for high phase purity zincblende GaN growth can be rather narrow.

IV. CONCLUSION

We have used the combination of HAADF STEM and ABF STEM to image the bonding configurations between Ga and N in a zb-GaN sample grown by MOVPE on vicinal (001) 3C-SiC/Si, which allowed us to correlate the miscut direction with the crystallographic [1-10] in-plane direction and to identify the polarity properties of the close-packed planes in the GaN thin film. It has been shown that the {111} planes viewed edge-on in the zone perpendicular to the miscut direction, namely, the [110] direction, have an N-polar character, whereas the {111} planes viewed edge-on in the [1-10] zone parallel to the miscut direction have Ga-polarity. These individual polarities are preserved at SFs by either rotating the coordination of N atoms or the coordination of Ga atoms by 180° around the ⟨111⟩ polar axes, respectively. We explained the observed formation of small amounts of the wurtzite phase on Ga-polar {111} planes of GaN and the total absence of evidence of these defective inclusions on N-polar {111} planes by the preferential growth of wz-GaN in the Ga-polar direction under non-optimized growth conditions.

SUPPLEMENTARY MATERIAL

See the supplementary material for the 3D-sketches of the atomic arrangement at Ga-polar and N-polar {111} intrinsic stacking faults in zb-GaN.

ACKNOWLEDGMENTS

AUTHOR DECLARATIONS

Conflict of Interest

The authors have no conflicts to disclose.

Author Contributions

Huixin Xiu, Simon M. Fairclough, and Martin Frentrup contributed equally to this work.

Huixin Xiu: Data curation (equal); Formal analysis (equal); Funding acquisition (equal); Investigation (equal); Visualization (equal); Writing – review & editing (equal). **Simon M. Fairclough:** Data curation (equal); Formal analysis (equal); Investigation (equal); Visualization (equal); Writing – review & editing (equal). **Abhiram Gundimeda:** Data curation (equal); Writing – review & editing (supporting). **Menno J. Kappers:** Writing – review & editing (equal). **David J. Wallis:** Funding acquisition (lead); Resources (equal); Writing – review & editing (supporting). **Rachel A. Oliver:** Resources (equal); Supervision (equal); Writing – review & editing (equal). **Martin Frentrup:** Formal analysis (equal); Investigation (equal); Supervision (equal); Visualization (equal); Writing – original draft (lead); Writing – review & editing (lead).

DATA AVAILABILITY

The data that support the findings of this study are available within the article and from the corresponding author upon reasonable request.

REFERENCES

[1]T. Hanada, "Basic properties of ZnO, GaN, and related materials," in *Oxide and Nitride Semiconductors—Processing, Properties, and Applications, Advances in Materials Research*, edited by T. Yao and S.-K. Hong (Springer, Berlin, 2009), Vol. 12.

[2]I. Vurgaftman and J. R. Meyer, J. Appl. Phys. **89**, 5815 (2001).

[3]V. D. Compeán-García, H. Moreno-García, E. López-Luna, H. Pérez Ladrón de Guevara, A. Escobosa Echavarría, Y. Kudriavtsev, F. J. Rodríguez-Aranda, A. G. Rodríguez, and M. A. Vidal, Mater. Sci. Semicond. Process. **93**, 196 (2019).

[4]C. A. Hernández-Gutiérre, Y. L. Casallas-Moreno, V.-T. Rangel-Kuoppa, D. Cardona, Y. Hu, Y. Kudriatsev, M. A. Zambrano-Serrano, S. Gallardo-Hernandez, and M. Lopez-Lopez, Sci. Rep. **10**, 16858 (2020).

[5]D. R. Elsaesser, M. T. Durniak, A. S. Bross, and C. Wetzel, J. Appl. Phys. **122**, 115703 (2017).

[6]E. Tschumak, R. Granzner, J. K. N. Lindner, F. Schwierz, K. Lischka, H. Nagasawa, M. Abe, and D. J. As, Appl. Phys. Lett. **96**, 253501 (2010).

[7]M. Abe, H. Nagasawa, S. Potthast, J. Fernandez, J. Schörmann, D. J. As, and K. Lischka, IEICE Trans. Electron **E89-C**, 1057 (2006).

[8]R. Granzner, E. Tschumak, M. Kittler, K. Tonisch, W. Jatal, J. Pezoldt, D. As, and F. Schwierz, J. Appl. Phys. **110**, 114501 (2011).

[9]H. Yang, O. Brandt, and K. Ploog, Phys. Status Solidi B **194**, 109 (1996).

[10]M. Frentrup, L. Y. Lee, S.-L. Sahonta, M. J. Kappers, F. Massabuau, P. Gupta, R. A. Oliver, C. J. Humphreys, and D. J. Wallis, J. Phys. D: Appl. Phys. **50**, 433002 (2017).

[11]L. Y. Lee, M. Frentrup, M. J. Kappers, R. A. Oliver, C. J. Humphreys, and D. J. Wallis, J. Appl. Phys. **124**, 105302 (2018).

[12]T. Lei, M. Fanciulli, R. J. Molnar, T. D. Moustakas, R. J. Graham, and J. Scanlon, Appl. Phys. Lett. **59**, 944 (1991).

[13]R. M. Kemper, P. Veit, C. Mietze, A. Dempewolf, T. Wecker, F. Bertram, J. Christen, J. K. N. Lindner, and D. J. As, Phys. Status Solidi C **12**, 469 (2015).

[14]S. A. Church, S. Hammersley, P. W. Mitchell, M. J. Kappers, S. L. Sahonta, M. Frentrup, D. Nilsson, P. J. Ward, L. J. Shaw, D. J. Wallis, C. J. Humphreys, R. A. Oliver, D. J. Binks, and P. Dawson, Phys. Status Solidi B **254**, 1600733 (2017).

[15]T. J. Wade, A. Gundimeda, M. J. Kappers, M. Frentrup, S. M. Fairclough, D. J. Wallis, and R. A. Oliver, "MOVPE studies of zincblende GaN on 3C-SiC/Si (001)," J. Cryst. Growth (unpublished).

[16]L. Y. Lee, M. Frentrup, P. Vacek, M. J. Kappers, D. J. Wallis, and R. A. Oliver, J. Appl. Phys. **125**, 105303 (2019).

[17]A. L. Allred, J. Inorg. Nucl. Chem. **17**, 215 (1961).

[18]M. Sumiya and S. Fuke, "Review of polarity determination and control of GaN". MRS Internet Journal of Nitride Semiconductor Research **9**, 1 (2004).

[19]F. A. Ponce, D. P. Bour, W. T. Young, M. Saunders, and J. W. Steeds, Appl. Phys. Lett. **69**, 337 (1996).

[20]B. Daudin, J. L. Rouvière, and M. Arlery, Appl. Phys. Lett. **69**, 2480 (1996).

[21]R. Dimitrov, M. Murphy, J. Smart, W. Schaff, J. R. Shealy, L. F. Eastman, O. Ambacher, and M. Stutzmann, J. Appl. Phys. **87**, 3375 (2000).

[22]K. Ueno, E. Kishikawa, J. Ohta, and H. Fujioka, APL Mater. **5**, 026102 (2017).

[23]C. I. Oppo, J. Malindretos, R. R. Zamani, D. Broxtermann, J. Segura-Ruiz, G. Martinez-Criado, P. C. Ricci, and A. Rizzi, Nanotechnology **27**, 355703 (2016).

[24]M. Sumiya, K. Yoshimura, K. Ohtsuka, and S. Fuke, Appl. Phys. Lett. **76**, 2098 (2000).

[25]D. Skuridina, D. V. Dinh, B. Lacroix, P. Ruterana, M. Hoffmann, Z. Sitar, M. Pristovsek, M. Kneissl, and P. Vogt, J. Appl. Phys. **114**, 173503 (2013).

[26]A. Roshko, M. D. Brubaker, P. T. Blanchard, K. A. Bertness, T. E. Harvey, R. H. Geiss, and I. Levin, J. Mater. Res. **32**, 936 (2017).

[27]F. Schuster, B. Laumer, R. R. Zamani, C. Magén, J. R. Morante, J. Arbiol, and M. Stutzmann, ACS Nano **8**, 4376 (2014).

[28]S. Y. Woo, M. Bugnet, H. P. T. Nguyen, Z. Mi, and G. A. Botton, Nano Lett. **15**(10), 6413 (2015).

[29]M. de la Mata, C. Magen, J. Gazquez, M. Iqbal Bakti Utama, M. Heiss, S. Lopatin, F. Furtmayr, C. J. Fernández-Rojas, B. Peng, J. R. Morante, R. Rurali, M. Eickhoff, A. Fontcuberta i Morral, Q. Xiong, and J. Arbiol, Nano Lett. **12**(5), 2579 (2012).

[30]P. Vacek, M. Frentrup, L. Y. Lee, F. C.-P. Massabuau, M. J. Kappers, D. J. Wallis, R. Gröger, and R. A. Oliver, J. Appl. Phys. **129**, 155306 (2021).

[31]M. Häberlen, T. J. Badcock, M. A. Moram, J. L. Hollander, M. J. Kappers, P. Dawson, C. J. Humphreys, and R. A. Oliver, J. Appl. Phys. **108**, 033523 (2010).

[32]J. Zúñiga-Pérez, V. Consonni, L. Lymperakis, X. Kong, A. Trampert, S. Fernández-Garrido, O. Brandt, H. Renevier, S. Keller, K. Hestroffer, M. R. Wagner, J. S. Reparaz, F. Akyol, S. Rajan, S. Rennesson, T. Palacios, and G. Feuillet, Appl. Phys. Rev. **3**, 041303 (2016).

[33]T. Matsuoka, Y. Kobayashi, H. Takahata, T. Mitate, S. Mizuno, A. Sasaki, M. Yoshimoto, T. Ohnishi, and M. Sumiya, Phys. Status Solidi B **243**, 1446 (2006).

[34]Q. Sun, Y. S. Cho, I.-H. Lee, J. Han, B. H. Kong, and H. K. Cho, Appl. Phys. Lett. **93**, 131912 (2008).